Research Article | Vol. 25, No. 26 | 25 Dec 2017 | OPTICS EXPRESS 33184
Optics EXPRESS

Partial Poincaré beams generated from wavelength-mismatched vortex plates

T. D. HUANG AND T. H. LU*

Department of Physics, National Taiwan Normal University, Taipei 11677, Taiwan
**thlu@ntnu.edu.tw*

Abstract: We propose a convenient method for generating partial Poincaré beams of light having space-variant polarization. The beams can be constructed from the incidence of the fundamental Gaussian beam with circular or linear polarization to a wavelength-mismatched vortex plate. The polarization state covers only a small portion of the surface of the Poincaré sphere, particularly, being visualized by some interesting close curves. We demonstrate that the partial Poincaré beam can be decomposed into different spatial modes with orthogonal polarizations. Numerical analyses of the vortex vector beam and the polarization distribution are consistent with experimental results. The partial Poincaré beams could supplement the concept and application of Full Poincare beams.

OCIS codes: (080.4865) Optical vortices; (260.5430) Polarization; (260.6042) Singular optics.

References and links

1. J. Wang, "Advances in communications using optical vortices," Photon. Res. **4**(5), B14–B28 (2016).
2. Q. Zhan, "Cylindrical vector beams: from mathematical concepts to applications," Adv. Opt. Photonics **1**(1), 1–57 (2009).
3. R. Dorn, S. Quabis, and G. Leuchs, "Sharper focus for a radially polarized light beam," Phys. Rev. Lett. **91**(23), 233901 (2003).
4. G. Unnikrishnan, M. Pohit, and K. Singh, "A polarization encoded optical encryption system using ferroelectric spatial light modulator," Opt. Commun. **185**(1-3), 25–31 (2000).
5. C.-J. Cheng and M.-L. Chen, "Polarization encoding for optical encryption using twisted nematic liquid crystal spatial light modulators," Opt. Commun. **237**(1-3), 45–52 (2004).
6. J. Yu, C. Zhou, L. Zhu, Y. Lu, J. Wu, and W. Jia, "Generalized non-separable two-dimensional Dammann encoding method," Opt. Commun. **382**, 539–546 (2017).
7. C. C. Sun and C. K. Liu, "Ultrasmall focusing spot with a long depth of focus based on polarization and phase modulation," Opt. Lett. **28**(2), 99–101 (2003).
8. L. Allen, M. W. Beijersbergen, R. J. C. Spreeuw, and J. P. Woerdman, "Orbital angular momentum of light and the transformation of Laguerre-Gaussian laser modes," Phys. Rev. A **45**(11), 8185–8189 (1992).
9. K. Yonezawa, Y. Kozawa, and S. Sato, "Generation of a radially polarized laser beam by use of the birefringence of a c-cut Nd:YVO_4 crystal," Opt. Lett. **31**(14), 2151–2153 (2006).
10. M. A. Ahmed, A. Voss, M. M. Vogel, and T. Graf, "Multilayer polarizing grating mirror used for the generation of radial polarization in Yb:YAG thin-disk lasers," Opt. Lett. **32**(22), 3272–3274 (2007).
11. C. S. Guo, S. J. Yue, X. L. Wang, J. Ding, and H. T. Wang, "Polarization-selective diffractive optical elements with a twisted-nematic liquid-crystal display," Appl. Opt. **49**(7), 1069–1074 (2010).
12. M. A. Ahmed, A. Voss, M. M. Vogel, and T. Graf, "Multilayer polarizing grating mirror used for the generation of radial polarization in Yb:YAG thin-disk lasers," Opt. Lett. **32**(22), 3272–3274 (2007).
13. T. H. Lu and L. H. Lin, "Observation of a superposition of orthogonally polarized geometric beams with a c-cut Nd:YVO_4 crystal," Appl. Phys. B **106**(4), 863–866 (2012).
14. T. H. Lu and C. H. He, "Generating orthogonally circular polarized states embedded in nonplanar geometric beams," Opt. Express **23**(16), 20876–20883 (2015).
15. P. Miao, Z. Zhang, J. Sun, W. Walasik, S. Longhi, N. M. Litchinitser, and L. Feng, "Orbital angular momentum microlaser," Science **353**(6298), 464–467 (2016).
16. X. L. Wang, J. Ding, W. J. Ni, C. S. Guo, and H. T. Wang, "Generation of arbitrary vector beams with a spatial light modulator and a common path interferometric arrangement," Opt. Lett. **32**(24), 3549–3551 (2007).
17. S. Zhou, S. Wang, J. Chen, G. Rui, and Q. Zhan, "Creation of radially polarized optical fields with multiple controllable parameters using a vectorial optical field generator," Photon. Res. **4**(5), B35–B39 (2016).
18. A. Forbes, A. Dudley, and M. McLaren, "Creation and detection of optical modes with spatial light modulators," Adv. Opt. Photonics **8**(2), 200–227 (2016).
19. M. Born and E. Wolf, *Principles of Optics* (Cambridge University, 1997).
20. G. Milione, H. I. Sztul, D. A. Nolan, and R. R. Alfano, "Higher-Order Poincaré Sphere, Stokes Parameters, and the Angular Momentum of Light," Phys. Rev. Lett. **107**(5), 053601 (2011).

#312745 https://doi.org/10.1364/OE.25.033184
Journal © 2017 Received 3 Nov 2017; revised 14 Dec 2017; accepted 14 Dec 2017; published 20 Dec 2017

Optics EXPRESS

21. E. J. Galvez, S. Khadka, W. H. Schubert, and S. Nomoto, "Poincaré-beam patterns produced by nonseparable superpositions of Laguerre-Gauss and polarization modes of light," Appl. Opt. **51**(15), 2925–2934 (2012).
22. F. Yue, D. Wen, C. Zhang, B. D. Gerardot, W. Wang, S. Zhang, and X. Chen, "Multichannel polarization-controllable superpositions of orbital angular momentum states," Adv. Mater. **29**(15), 1603838 (2017).
23. Y. Liu, X. Ling, X. Yi, X. Zhou, H. Luo, and S. Wen, "Realization of polarization evolution on higher-order Poincaré sphere with metasurface," Appl. Phys. Lett. **104**(19), 191110 (2014).
24. Z. Liu, Y. Liu, Y. Ke, Y. Liu, W. Shu, H. Luo, and S. Wen, "Generation of arbitrary vector vortex beams on hybrid-order Poincaré sphere," Photon. Res. **5**(1), 15 (2017).
25. X. Yi, Y. Liu, X. Ling, X. Zhou, Y. Ke, H. Luo, S. Wen, and D. Fan, "Hybrid-order Poincaré sphere," Phys. Rev. A **91**(2), 023801 (2015).
26. A. M. Beckley, T. G. Brown, and M. A. Alonso, "Full Poincaré beams," Opt. Express **18**(10), 10777–10785 (2010).
27. Z. Liu, Y. Liu, Y. Ke, J. Zhou, Y. Liu, H. Luo, and S. Wen, "Geometric phase Doppler effect: when structured light meets rotating structured materials," Opt. Express **25**(10), 11564–11573 (2017).
28. L. Marrucci, C. Manzo, and D. Paparo, "Optical Spin-to-Orbital Angular Momentum Conversion in Inhomogeneous Anisotropic Media," Phys. Rev. Lett. **96**(16), 163905 (2006).

1. Introduction

Numerous studies have investigated optical beams of scalar and vector fields for applications in optical communications [1,2], high-resolution imaging [3], optical encryption [4–6], and tight focusing methods [7]. Optical scalar fields are associated with the spatial structure of beams, and the phase distribution of scalar fields reveals the characteristics of the optical orbital angular momentum (OAM) [8]. By contrast, optical vector fields are related to light's polarization structure, and the specific handiness of the polarization demonstrates the spin angular momentum. The merit of vector beams is linked to their interaction with materials and potential application for optical manipulation. Several methods can be employed to generate spatially-variant vector beams, including bulk intracavity systems [9], polarization-selective devices [10,11], compact laser designs [12–15], and spatial light modulator systems [16–18]. The states of polarization of spatially-variant vector beams can be described with Stokes parameters and mapped onto the Poincaré sphere [19].

The Laguerre-Gaussian eigenmodes of OAM beams with opposite circular polarization and topological charges have been superimposed onto the high-order Poincaré sphere [20,21]. Recently, the metasurface is used to realize vector OAM superposition, and the polarization states can be mapped onto the high-order Poincare sphere [22,23]. For a more general form, the beam with two different OAM states can be described with the hybrid-order Poincaré sphere [24,25]. However, superimposing a fundamental Gaussian mode and an OAM mode having orthogonal circular polarizations extended the states of polarization coverage on the full Poincaré sphere [26]. The full Poincaré beam can be demonstrated by exploiting the stress birefringence distribution present in a stressed optical element or using the wavelength-matched vortex plate [27]. Nevertheless, investigating what occurs under the wavelength-mismatched condition is valuable because it offers an alternative method for generating partial Poincaré beams.

In this work, we propose a convenient approach for using a wavelength-mismatched vortex plate to generate a new type of a vector beam with spatially-variant polarization states that can be mapped onto a part of the Poincaré sphere. Different from a q-plate which uses voltage to control the phase retardation for variable wavelength, the vortex plate is a fixed phase retarder for a given wavelength with no voltage. For a commercial vortex plate product, the incident Gaussian beam with circular polarization can be transformed to a high-order Laguerre-Gaussian mode with opposite circular polarization for a specific wavelength. However, we used a Gaussian beam of mismatched wavelength incident to a vortex plate. Light with a wavelength of 1064 nm is incident to the conventional vortex plate with half-wave retardation designed for light with a wavelength of 532 nm. After passing through the vortex plate, the resulting beam is the superposition of fundamental Gaussian mode and the high-order Laguerre-Gaussian mode with orthogonal circular polarization. The incident beams of different polarization states lead to an output beam with different spatial intensities

Optics EXPRESS

and polarization distributions. The conventional vortex plates and light with a mismatched wavelength could be combined to generate various vectorial vortex beams. Comparing with the full Poincaré beams, we use vortex plates to generate the partial Poincaré beams with polarization states mapped onto the equator and a closed curve of the Poincaré sphere.

2. Theory

We used Jones vector and Jones matrix to represent the polarized beam and the transformation process of the optical element. Let $\mathrm{T}(\mathrm{x},\mathrm{y})$ v represents the transformation matrix of the vortex plate. The transformation matrix is the same as the matrix of q-plates and consists of two rotation matrices by angle θ and the phase retardation matrix [28]. Subsequently,

$$\mathrm{T}(\mathrm{x},\mathrm{y},\theta,\varphi)=\begin{pmatrix}\cos\theta & -\sin\theta\\ \sin\theta & \cos\theta\end{pmatrix}\begin{pmatrix}t_x & 0\\ 0 & t_y\cdot e^{i\varphi}\end{pmatrix}\begin{pmatrix}\cos\theta & \sin\theta\\ -\sin\theta & \cos\theta\end{pmatrix} \tag{1}$$

where $\theta=q\phi+\delta$ is the orientation of the fast axis at a given azimuthal angle ϕ on the waveplate and δ is the orientation of the fast axis at $\phi=0$. t_x, t_y are the transmission coefficients for light polarized parallel and perpendicular to the fast axes, and φ is the retardation of the vortex plate. In this work, we set $t_x=t_y=1$ and $\delta=0$. The typical vortex plates were designed as vortex half-wave plates, and the retardation φ equaled π. We used Dirac bra-ket notation to simplify the representation of the incident and transformed output beams. The transformation of the output beam of the incident light into a half-wave vortex plate can be written as follows:

$$|E_{out}\rangle=\mathrm{T}(\mathrm{x},\mathrm{y},\theta,\pi)|E_{in}\rangle=e^{i2q\phi}|R\rangle\langle L|E_{in}\rangle+e^{-i2q\phi}|L\langle R|E_{in}\rangle \tag{2}$$

where $|R\rangle=(1,-i)^T/\sqrt{2}$ and $|L\rangle=(1,i)^T/\sqrt{2}$. Obviously, the incident Gaussian beam with circular polarization can be transformed into a vortex beam with $\pm 2q$ topological charge and opposite circular polarization. The phase retardation of the vortex plate can be described as $2\pi(n_e-n_o)d/\lambda$, where d is the depth of the vortex plate and λ is the wavelength of the incident light. When the wavelength of the incident beam was twice the originally designed wavelength for the vortex half-wave plate, the retardation of the vortex plate was approximately $\pi/2$. The vortex plate was regarded as the mismatched vortex plate in this condition. The transformed output beam can be written as

$$|E_{out}\rangle=\mathrm{T}(\mathrm{x},\mathrm{y},\theta,\pi/2)|E_{in}\rangle=\alpha|E_{in}\rangle+\beta\left(e^{i2q\phi}|R\langle L|E_{in}\rangle+e^{-i2q\phi}|L\rangle\langle R|E_{in}\rangle\right) \tag{3}$$

where $\alpha=(1+i)/2$ and $\beta=(1-i)/2$. The first part should maintain the original polarization and phase of the incident beam. In this study, the main stress fell on the incident Gaussian beams with left circular, right circular, and linear polarization passing through the mismatched vortex plate. Consider the incident light as $|E_{in}\rangle=\mathrm{LG}_{0,0}|R\rangle$, $\mathrm{LG}_{0,0}|L\rangle$, and $\mathrm{LG}_{0,0}|H\rangle$ where $\mathrm{LG}_{p,\ell}$ represents Laguerre-Gaussian mode with radial index p and azimuthal index ℓ. The output beams can be described as

$$|E_{out}\rangle=\alpha\cdot\mathrm{LG}_{0,0}|R\rangle+\beta\cdot\mathrm{LG}_{0,-2q}|L\rangle, \tag{4}$$

$$|E_{out}\rangle=\alpha\cdot\mathrm{LG}_{0,0}|L\rangle+\beta\cdot\mathrm{LG}_{0,2q}|R\rangle, \tag{5}$$

and

Optics EXPRESS

$$\left|E_{out}\right\rangle = (\alpha \cdot \mathrm{LG}_{0,0} + \beta \cdot \mathrm{LG}_{0,2q})\left|R\right\rangle + (\alpha \cdot \mathrm{LG}_{0,0} + \beta \cdot \mathrm{LG}_{0,-2q})\left|L\right\rangle, \quad (6)$$

respectively. The parameters α and β denote weighting coefficients of the incident beam and vortex beam.

3. Experimental setup and results

The use of vortex plates to create both spin angular momentum and OAM has been described in detail. We built an experiment based on the mismatched vortex plate to generate vector vortex beams. The experimental setup is shown in Fig. 1. Light with a 1064 nm wavelength emitted from a diode-pumped solid state laser was sent to a polarizer and a quarter-wave plate to manipulate the polarization state of input fundamental Gaussian beams passing through the vortex plate. The fast-axis orientation of the vortex plate (vortex half-wave retarders for 532 nm, Thorlabs Company) is shown in Fig. 1. The vortex plate caused the incident Gaussian beam with spatially homogeneous polarization to be converted into a vortex beam with spatially inhomogeneous polarization. The vortex plate was used as the wavelength-mismatched vortex plate. The second quarter-wave plate and polarizer were utilized to analyze the polarization states of output vector beams. The intensity profiles were captured using a charge-coupled device camera.

The conventional vortex plate that was used as a vortex half-wave retarder could convert the circular polarization $\mathrm{LG}_{0,0}$ mode to the $\mathrm{LG}_{0,\pm 2q}$ mode with opposite handed circular

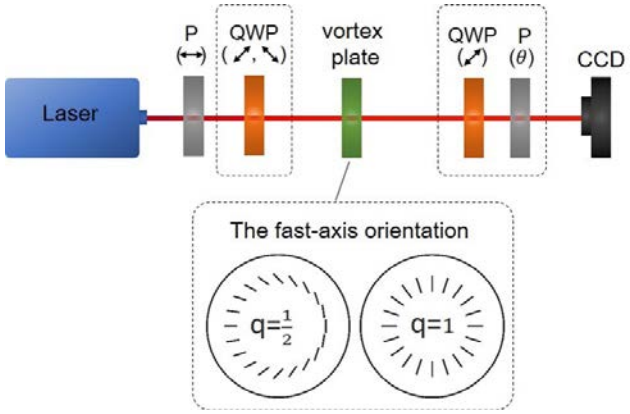

Fig. 1. Experimental setup for generating and analyzing a partial Poincaré sphere beam and the distribution of the fast-axis orientation of the vortex plates. P: polarizer, QWP: quarter wave plate.

polarization. In this study, the wavelength-mismatched vortex plate could convert one part of the $\mathrm{LG}_{0,0}$ mode to the $\mathrm{LG}_{0,\pm 2q}$ mode with opposite handed circular polarization and keep the other part unconverted. This is a simple method for generating a vector vortex beam with hybrid orders. A right circularly polarized Gaussian beam generated by being passed through a polarizer of horizontal orientation and a quarter-wave plate of 45^{o} orientation was incident to a mismatched vortex plate ($q = 1/2$). Figure 2(a) depicts the intensity profile of the vector vortex beam and the polarization-resolved results with the beam passing through the analyzer that comprises a quarter-wave plate of 45^{o} orientation and a polarizer with different orientations. The results of the horizontal and vertical polarizer indicated that the orthogonal bases (right and left circular polarization) of the vector beam were the $\mathrm{LG}_{0,-1}$ and $\mathrm{LG}_{0,0}$ modes. Figure 2(b) shows the condition of the incident beam of left circular polarization. It is a complementary condition compared with the condition shown in Fig. 2(a). Figure 2(c)

Optics EXPRESS

shows the condition of the incident beam of linear polarization. It can be considered the combination

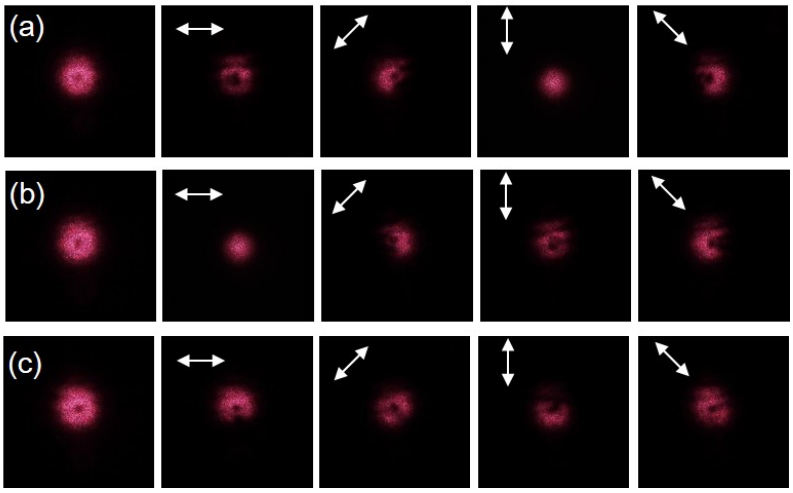

Fig. 2. Intensity distribution of the experimental results of vector beams generated from the vortex plate ($q = 1/2$) by the incident of Gaussian beams with different polarizations. The input Gaussian beam is: (a) right circularly polarized beam, (b) left circularly polarized beam, and (c) linearly polarized beam. The two to five columns show the polarization-resolved patterns for the vector beams passing through a quarter-wave plate and a polarizer. The arrow direction indicates the orientation of the polarizer.

of the right and left circularly polarized incident beams. The polarization-resolved results indicated that the orthogonal bases of the output vector beam were related to the superposition of the fundamental Gaussian mode $LG_{0,0}$ and Laguerre-Gaussian modes with opposite topological charge $LG_{0,\pm 2q}$. The output beams shown in the first column of Fig. 2 are similar in their intensity profiles but are completely different in the embedded polarization states.

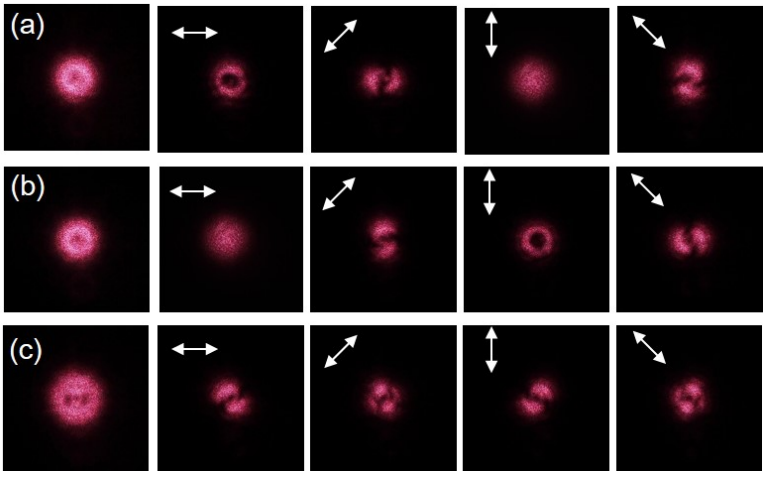

Fig. 3. The intensity distribution of the experimental results of vector beams generated from the vortex plate ($q = 1$) by the incident of Gaussian beams with different polarizations. The input Gaussian beam is: (a) right circularly polarized beam, (b) left circularly polarized beam, and (c) linearly polarized beam. The two to five columns show the polarization-resolved patterns for the vector beams passing through a quarter-wave plate and a polarizer. The arrow direction indicates the orientation of the polarizer.

Optics EXPRESS

Figure 3 reveals the intensity profiles and the polarization-resolved results of the output vector beams corresponding to the left circular, right circular, and linear polarization input beams incident to the mismatched vortex plate ($q = 1$). Based on the polarization-resolved patterns, the output vector beams can be clearly projected onto the orthogonal bases. The results of the horizontal and vertical polarizer shown in Fig. 3(a) indicated that the orthogonal bases (right and left circular polarization) of the vector beam were the $LG_{0,-2}$ and $LG_{0,0}$ modes. The first two rows show the results of the complementary cases of opposite circularly polarized input beams. For a linear polarized beam incident to the mismatched vortex plate, the corresponding output vector beam is more complicated than the vector beam generated from the conventional vortex plate. The intensity profiles related to the horizontal and vertical polarizer shown in Fig. 3(c) reveal that orthogonal bases are the superposed wave function $LG_{0,-2} + LG_{0,0}$ with left circular polarization and $LG_{0,2} + LG_{0,0}$ with right circular polarization. The characteristics of patterns included two spiral arms depending on the difference in azimuthal orders.

4. Numerical results

According to the theoretical analyses of the mismatched vortex plate, the analyses of numerical intensities under different polarizations are shown in Fig. 4 corresponding to the experimental results in Fig. 2. Figures 4(a)–4(c) illustrate the right and left circularly and linearly polarized Gaussian beams incident to the mismatched vortex plate ($q = 1/2$), and the output vector vortex beams are represented in Eqs. (4)–(6) with parameters $\alpha = \beta = 0.5$, respectively. We used the Jones matrix to analyze the superposed vector beams passing through the combination of a quarter-wave plate and a polarizer with different directions. Moreover, Fig. 5 shows the numerical results of three types of polarized Gaussian beams incident to the mismatched vortex plate ($q = 1$) corresponding to the experimental results shown in Fig. 3. The parameters α and β equal 0.5. The analyses of numerical intensities under different polarizations help explain the experimental polarization-resolved patterns and exhibit favorable agreement with the experimental results.

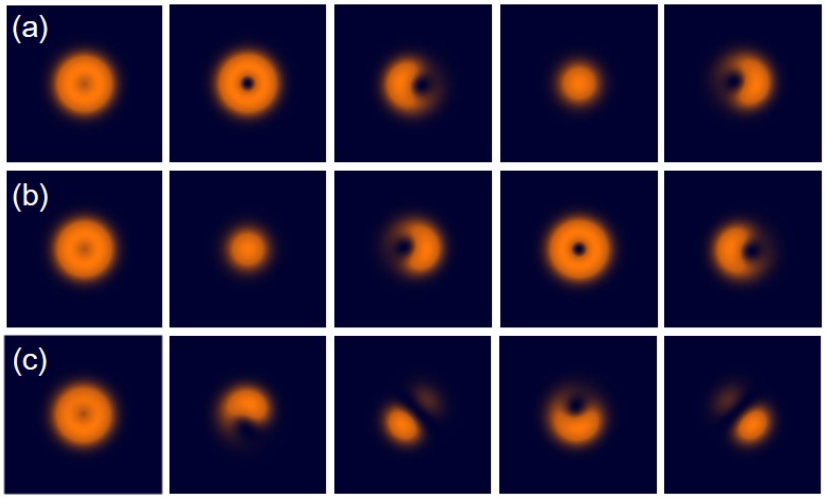

Fig. 4. The intensity distribution of the theoretical results corresponding to the experimental results shown in Fig. 2.

Optics EXPRESS

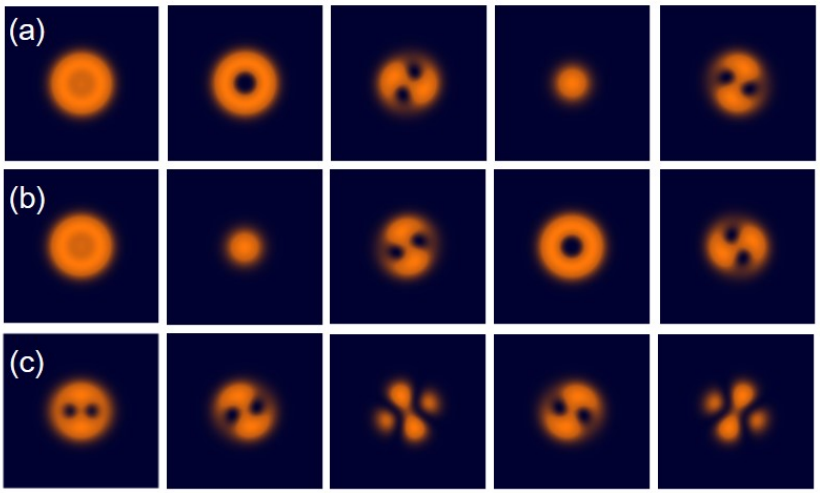

Fig. 5. The intensity distribution of the theoretical results corresponding to the experimental results shown in Fig. 3.

To analyze polarization states embedded in the vortex beam, a polarizer was used to examine the polarization of light passing through the mismatched vortex plate. Figure 6(b) shows the polarization-resolved patterns generated from the vortex plate ($q = 1/2$) with the input beam of right circular polarization. The arrow indicates the transmission axis of the polarizer. The bottom left of Fig. 6(b) illustrates the polarization distribution of the vortex beam.

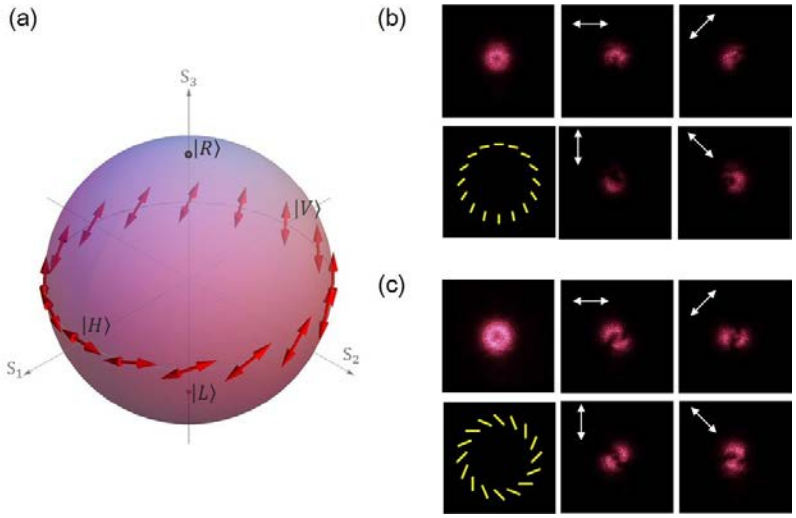

Fig. 6. (a) Schematic diagram of the Poincaré sphere. The red arrows depict the linear polarization states on the equator of the Poincaré sphere. (b) The top left shows the vector beam generated from the vortex plate ($q = 1/2$) with the input right circularly polarized Gaussian beam. The bottom left shows the polarization distribution. The polarization resolved patterns depict the vector beam passing through an orientated polarizer. The polarization states can be mapped onto the equator of the Poincaré sphere. (c) The top left shows the vector beam generated from the vortex plate ($q = 1$) with the input right circularly polarized Gaussian beam. The bottom left shows the polarization distribution. The polarization-resolved patterns depict the vector beam passing through an orientated polarizer. The polarization states can be mapped onto the equator two rounds of the Poincaré sphere.

Optics EXPRESS

Figure 6(c) demonstrates the polarization-resolved results for the condition of the vortex plate of $q = 1$. Briefly, the mismatched vortex plate in this condition can be regarded as the vortex quarter-wave retarder because the wavelength of the input light was twice as large than the designed wavelength for the vortex plate. Consequently, the input light of circular polarization incident to the quarter-wave retarder vortex plate was transformed to the vortex beam with space-variant linear polarization. The orientation of the linear polarization of the vector beam is 45^{o} with respect to the orientation of the fast axis of the vortex plate shown in Fig. 1. Any polarized states can be mapped onto the Poincaré sphere. Figure 6(a) depicts the Poincaré sphere and the orientation of linearly polarized states on the equator. For a right circularly polarized Gaussian light incident to a mismatched vortex plate, the experimental results revealed that the polarized state mapped onto the Poincaré sphere. The polarized states embedded in the vortex vector beam generated from the vortex plate with $q = 1/2$ just filled the equator. The transformation of the polarization states can be regarded as traversing from the north pole to the equator with different paths. Furthermore, the polarized states embedded in the vortex vector beam generated from the vortex plate with $q = 1$ also filled the equator. Each position on the equator represents two polarized states of the vortex vector beam. Let us consider the subject from the input Gaussian beam with linear polarization. Figure 7(b) shows the polarization-resolved patterns generated from the mismatched vortex plate ($q = 1/2$) with the input beam of linear polarization. The arrow indicates the transmission axis of the polarizer. According to the polarization-resolved results from Figs. 2 and 7(b), the polarization distribution of the vortex vector beam could be reconstructed and is illustrated in the bottom left of Fig. 7(b). The mismatched vortex plate was used as the quarter-wave vortex plate, so the polarization states can be transformed from linear polarization to circular or elliptical polarization corresponding to the orientation of the fast-axis shown in Fig. 1.

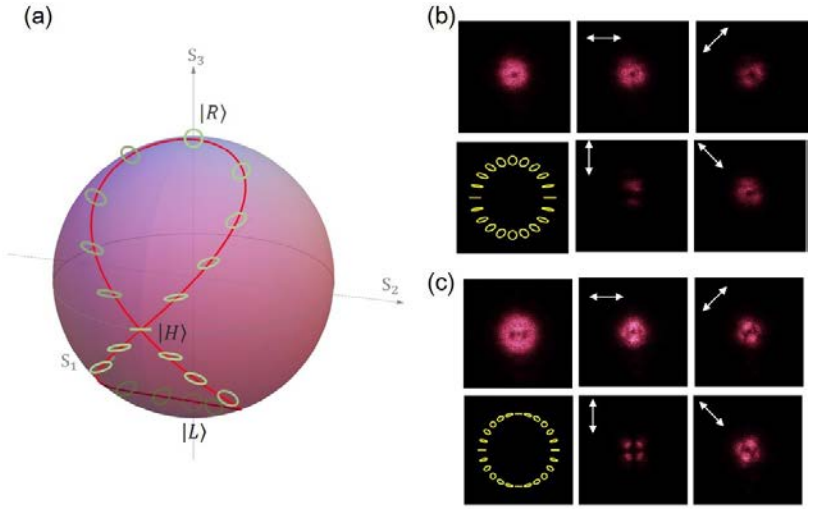

Fig. 7. (a) Schematic diagram of the Poincaré sphere. The green figures depict the polarization states on the red curve of the Poincaré sphere. (b) The top left shows the vector beam generated from the vortex plate ($q = 1/2$) with the input linearly polarized Gaussian beam. The bottom left shows the polarization distribution. The polarization-resolved patterns depict the vector beam passing through an orientated polarizer. The polarization states can be mapped onto the red curve of the Poincaré sphere shown in (a). (c) The top left shows the vector beam generated from the vortex plate ($q = 1$) with the input linearly polarized Gaussian beam. The bottom left shows the polarization distribution. The polarization-resolved patterns depict the vector beam passing through an orientated polarizer. The polarization states can be mapped onto the red curve two rounds of the Poincaré sphere shown in (a).

Optics EXPRESS

Figure 7(c) demonstrates the polarization-resolved results for the vortex plate where $q = 1$. For a linearly polarized Gaussian beam incident to a quarter-wave vortex plate, the polarized state can be mapped on the Poincaré sphere. Figure 7(a) depicts that the polarization distribution of the vortex vector beam was projected onto the Poincaré sphere and formed a curve. The transformation of the polarization states can be regarded as traversing from one point of the equator to other points on the curve in one round and two rounds corresponding to the vortex plates where $q = 1/2$ and 1. The polarization states of the vectorial vortex beam can be described by Eq. (6). Notably, when illuminated with linearly polarized light, such light beams could comprise three different OAM modes, which is beyond two-dimensional thinking with the matched vortex plate.

The measurement of the Stokes parameters is an effective approach to analyze the polarization states [19-20, 23]. In the experimental setup, we can measure the Stokes parameters from the optical intensities recorded by the camera. However low power and large divergence of the input laser beam of 1064 nm lead to the imperfect optical images in the experimental results. In the experimental setup, a diaphragm was used in front of the camera to block the ineffective light with large divergence. The resolution and contrast of the Stokes parameters are not good enough to reconstruct the polarization states of the optical modes in present condition. The improvement of beam quality of the input laser beam helps to get better image quality and makes it possible to analyze the precise polarization states at each point of the beam section. We leave the details for future work when we consider complex high-order vector beams.

5. Conclusion

We have demonstrated partial Poincaré beam generation by exploiting the polarized fundamental Gaussian beam incident to the wavelength-mismatched vortex plate. The partial Poincaré beam was decomposed into different OAM beams with orthogonal circular polarization states. The experimental vectorial vortex beams exhibited favorable agreement with the theoretical analysis and numerical results. The compact experimental approach may find potential applications in optical manipulation and offers a new angle to understand the spin-orbit interaction of light.

Funding

This work is supported by the Ministry of Science and Technology of Taiwan (Contract No. MOST105-2112-M-003-009).

Acknowledgments

We gratefully acknowledge helpful discussions from Professor Lixiang Chen at Xiamen University.